

Cross-attention learning enables real-time nonuniform rotational distortion correction in OCT

HAORAN ZHANG¹, JIANLONG YANG^{1,*}, JINGQIAN ZHANG¹, SHIQING ZHAO¹, AND AILI ZHANG¹

¹ School of Biomedical Engineering, Shanghai Jiao Tong University, Shanghai, China
 *jyangoptics@gmail.com

Compiled June 8, 2023

Nonuniform rotational distortion (NURD) correction is vital for endoscopic optical coherence tomography (OCT) imaging and its functional extensions, such as angiography and elastography. Current NURD correction methods require time-consuming feature tracking or cross-correlation calculations and thus sacrifice temporal resolution. Here we propose a cross-attention learning method for the NURD correction in OCT. Our method is inspired by the recent success of the self-attention mechanism in natural language processing and computer vision. By leveraging its ability to model long-range dependencies, we can directly obtain the correlation between OCT A-lines at any distance, thus accelerating the NURD correction. We develop an end-to-end stacked cross-attention network and design three types of optimization constraints. We compare our method with two traditional feature-based methods and a CNN-based method, on two publicly-available endoscopic OCT datasets and a private dataset collected on our home-built endoscopic OCT system. Our method achieved a $\sim 3\times$ speedup to real time (26 ± 3 fps), and superior correction performance.

<http://dx.doi.org/10.1364/ao.XX.XXXXXX>

Optical coherence tomography (OCT) is an *in vivo* imaging modality with near-cellular spatial resolution. Its clinical application scope of OCT is expanding from ophthalmology to other fields, such as cardiovascular, respiratory, gastrointestinal, and cervical [1]. For such applications, an endoscopic probe with point-by-point scanning capability is required. Typically, the scanning is controlled externally and implemented mechanically to achieve axial movement and circumferential rotation of the probe (referred to as proximal scanning). In recent years, with the development of technologies such as MEMS and piezoelectric devices, point-by-point scanning can be achieved by shifting the beam at the output end of the probe (referred to as distal scanning). However, the distal scanning is currently rarely used clinically due to its significantly higher cost and larger size of the probe compared to the proximal scanning [2].

Due to the irregularities in the shape of vessels and other lumen structures, friction, and torque transmission losses, the rotation of the proximal scanning probe becomes non-uniform,

resulting in distortion of the intracanal OCT images, known as non-uniform rotational distortion (NURD). NURD can introduce errors in the morphological representation of tissues and make it difficult to perform functional imaging of tissue, such as elasticity, birefringence, angiography, and treatment processes [3–5].

Existing methods for the NURD correction are primarily based on feature tracking and cross-correlation [5, 6], which are time-consuming. Other methods utilize hardware and prior knowledge specific to the imaging target [3, 7], thus lacking generality. Uribe-Patarroyo and Bouma developed a method based on speckle decorrelation [8], which could perform NURD correction in real time, but the decorrelation is vulnerable to the variation of environment, such as motion and temperature [9]. Recently, Liao *et al.* proposed a convolutional neural network (CNN)-based learning method for the NURD correction [10]. Their methods outperformed previous ones on correction performance and achieved a processing rate of around 7 fps. However, CNNs have limitations in modeling long-range dependencies due to the constraints of local receptive fields and fixed convolutional kernel sizes, thus require to pre-build a correlation matrix, which affects their capability to scale up the processing efficiency.

In this Letter, we propose a cross-attention learning method to address the limitations above. Our method is inspired by the recent success of the self-attention mechanism [11] in natural language processing and computer vision, which has played a crucial role in the development of cutting-edge tools like ChatGPT [12]. Our key finding here is that the self-attention mechanism enables the direct establishment of global correlations within OCT A-line sequences, without the necessity of correlation calculation in advance. Because the self-attention mechanism is used between different A-lines, we refer to it here as cross-attention. For achieving a high correction efficiency, we develop an end-to-end stacked cross-attention network and design three types of optimization constraints.

Figure 1 presents a comparison between the results of our proposed method and three other representative approaches, including two feature-based methods [5, 6] (referred to as DP and FT, respectively) and the CNN-based method in [10] (referred to as De-NURD). Two public endoscopic OCT datasets [13, 14] and a private dataset collected on our home-built endoscopic OCT system are used in this evaluation. Orange bars are their standard deviation (STD), which is commonly used to represent

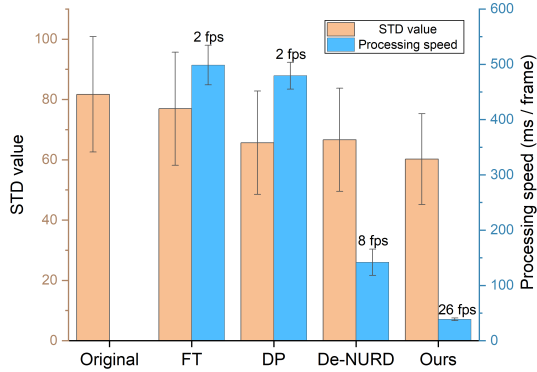


Fig. 1. Comparison between the results of our proposed method and three other representative approaches, including two feature-based methods [5, 6] (referred to as DP and FT, respectively) and the CNN-based method in [10] (referred to as De-NURD).

the correction performance (smaller means better) [6, 10]. Blue bars are the processing speed (ms/frame) and the corresponding frame rate in fps. It can be observed that our method achieves the best correction performance while also improving processing speed by about three times, reaching real-time performance.

Figure 2 illustrates the overall framework of our proposed

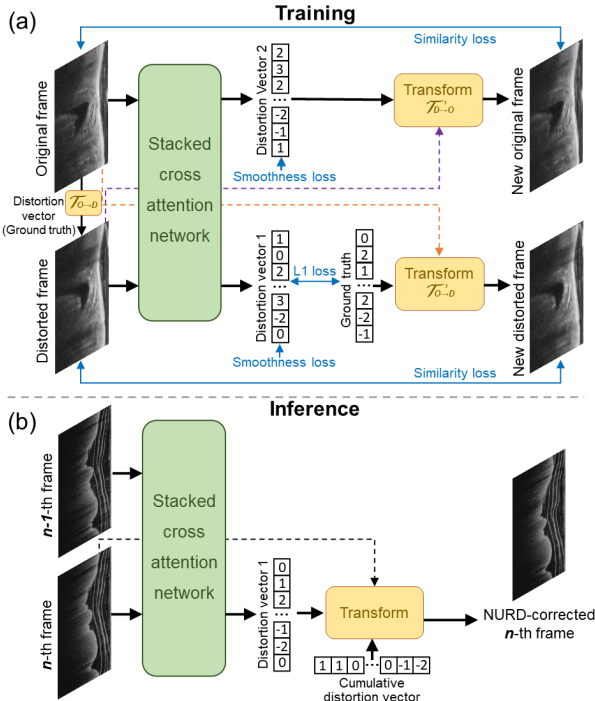


Fig. 2. Overall framework of our proposed method. (a) and (b) illustrate its training and inference phases, respectively.

method. (a) and (b) illustrate its training and inference phases, respectively. We use a self-supervised generative learning approach for training, *i.e.*, by distorting the original B-scans and then using the network to predict their distortions. Specifically, in Fig. 2, we use a distortion vector, which serves as the ground truth (GT) of the A-line shifts due to the NURD, to do the transform $T_{O \rightarrow D}$ from the original frame to the distorted frame (the

generation of the GT distortion vectors follows the method described in Section 3.2.1 of [10]). These two frames are then fed into the stacked cross-attention network, which is employed to correct the NURD. It predicts two distortion vectors: the first one is the distortion applied on the original frame to form the distorted frame; the second one is the distortion applied on the distorted frame to form the original frame. This design is inspired by the notion of cycle consistency in generative learning [15]. We found it improves the correction performance as shown in the results below. Using these predicted vectors, we can apply the transform $T'_{O \rightarrow D}$ and $T'_{D \rightarrow O}$ to the original and distorted frames, and form the new distorted and original frames, respectively. We use three types of optimization constraints in the training: (1) mean absolute error loss (L1 loss) between the distortion vector 1 and the GT vector, (2) smoothness loss of the predicted distortion vectors, and (3) similarity losses between the original/distorted frames and the new original/distorted frames at the A-line level. We list their functions below:

$$\mathcal{L}_1 = \frac{1}{N} \sum_{i=1}^N |\hat{d}_i - d_i|, \quad (1)$$

$$\mathcal{L}_{smoothness} = \frac{1}{N-1} \sum_{i=1}^{N-1} |\hat{d}_i - \hat{d}_{i+1}|, \quad (2)$$

$$\mathcal{L}_{similarity} = \frac{1}{N} \sum_{i=1}^N \left| \frac{1}{M} \sum_{j=1}^M \hat{p}_{i,j} - \frac{1}{M} \sum_{j=1}^M p_{i,j} \right|, \quad (3)$$

where \hat{d}_i and d_i are the elements of the predicted distortion vector and ground truth, respectively. N is the length of the vector (also the number of A-lines in each frame). M is the number of data points in each A-line. $\hat{p}_{i,j}$ and $p_{i,j}$ are the pixel value of data point j in A-line i from the predicted new frame and the corresponding input image, respectively.

In the inference phase, two successively acquired OCT B-scans (the $n-1$ -th and n -th frames. n refers to time points) are fed into the trained stacked cross-attention network. This is under the assumption that these two frames exhibit a high degree of morphological consistency, which is valid for current endoscopic OCT systems with an A-line rate of above 50 kHz [1, 2]. The output of this network is only the distortion vector 1, which is used to correct the NURD of the n -th frame. For the continuously acquired OCT B-scan sequence, we also consider the impact of NURD correction errors in the previous frames on the correction of the n -th frame. We generate the cumulative distortion vector using the method described in [10]. Both vectors are applied to get the NURD-corrected n -th frame.

Figure 3 illustrates the stacked cross-attention network. (a) is the overall architecture and (b) is the details of the multi-head cross-attention module. Instead of 2D operations employed in CNNs, here we use each A-line (1D) of the OCT B-scans as a token. Then they are used to calculate the query (Q), key (K), and value (V) vectors in the self-attention mechanism [11]:

$$Q = X \cdot W_Q + b_Q \quad (4)$$

$$K = X \cdot W_K + b_K \quad (5)$$

$$V = X \cdot W_V + b_V \quad (6)$$

where X ($X \in \mathbb{R}^{N \times M}$) is the input tokens with N A-lines and M data points in each A-line. The linear projection is defined as: $Q, K, V \in \mathbb{R}^{N \times E}$ (E is the embedding dimension, and $E > M$), and W_Q, W_K, W_V are weight matrices, while b_Q, b_K, b_V are bias terms. This linear projection step allows the model

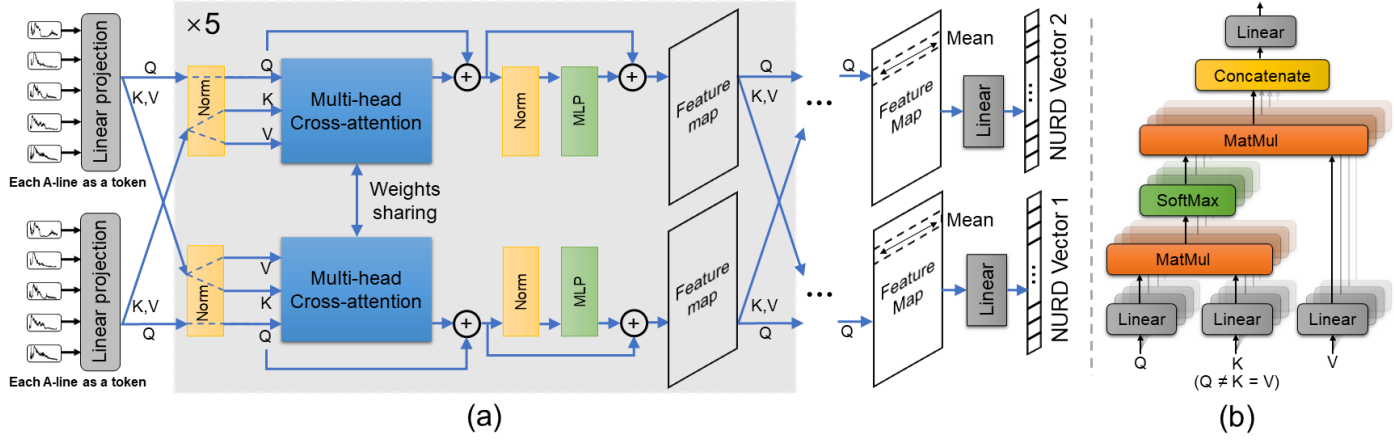


Fig. 3. Illustration of the stacked cross-attention network. (a) is the overall architecture and (b) is the details of the multi-head cross-attention module.

to capture different aspects of the input sequence. The query vectors \mathbf{Q} represent the current token and are responsible for computing attention weights. The key vectors \mathbf{K} capture the contextual information of each element, enabling the model to assess the relevance between different elements. The value vectors \mathbf{V} carry the actual content information associated with each token. Then these vectors are fed into 5 consecutive multi-head cross-attention blocks ($\times 5$). Each block includes a multi-head cross-attention module and a multi-layer perception (MLP) module [11]. In each block, we apply layer normalization (Norm) before each module and conduct residual connections. Finally, we perform averaging and linear operations to get the distortion vectors.

The multi-head cross-attention module in Fig. 3(b) allows the model to attend to different parts of the input sequence and capture diverse dependencies, enhancing its representation and predictive capabilities. Given a sequence of input embeddings $\mathbf{X} = [\mathbf{x}_1, \mathbf{x}_2, \dots, \mathbf{x}_n]$, the output is computed as follows:

$$\text{MultiHead}(\mathbf{Q}, \mathbf{K}, \mathbf{V}) = \text{Concat}(\text{head}_1, \text{head}_2, \dots, \text{head}_h) \mathbf{W}^O \quad (7)$$

where $\text{head}_i = \text{Attention}(\mathbf{QW}_i^Q, \mathbf{KW}_i^K, \mathbf{VW}_i^V)$ represents the attention mechanism applied on the projected queries \mathbf{QW}_i^Q , keys \mathbf{KW}_i^K , and values \mathbf{VW}_i^V of the i -th attention head. Here, \mathbf{W}_i^Q , \mathbf{W}_i^K , and \mathbf{W}_i^V are learnable linear projection matrices specific to each attention head. The concatenated outputs are then linearly transformed by the matrix \mathbf{W}^O to produce the final output.

We implement the code of our proposed method using PyTorch. Our model is trained on a personal computer with an Nvidia 3090 GPU (24G onboard memory). We convert an endoscopic OCT B-scan into an input format where each frame consists of 1024 A-lines, and each A-line contains 512 data points. We employ the multi-head cross-attention with an embedding dimension of 1024 and 4 heads. We use the SGD optimizer with a learning rate of $5e-4$. We set a batch size of 24 and train our model for 200 epochs. As mentioned above, we use the STD $\sigma(n)$ to quantitatively evaluate the correction performance [6]:

$$\sigma(n) = \frac{1}{N \times M} \sum_{i=1, j=1}^{N \times M} \tilde{\sigma}_5(p_{i,j}) \quad (8)$$

where $\tilde{\sigma}_5(p_{i,j})$ is the STD of pixel $p_{i,j}$ in adjacent 5 frames with n -th frame as the center. Precise correction can reduce the STD

to nearly 0, but it will never be exactly 0 due to variations in scanning locations and speckle noise.

We collect a total of 7,731 endoscopic OCT B-scans from

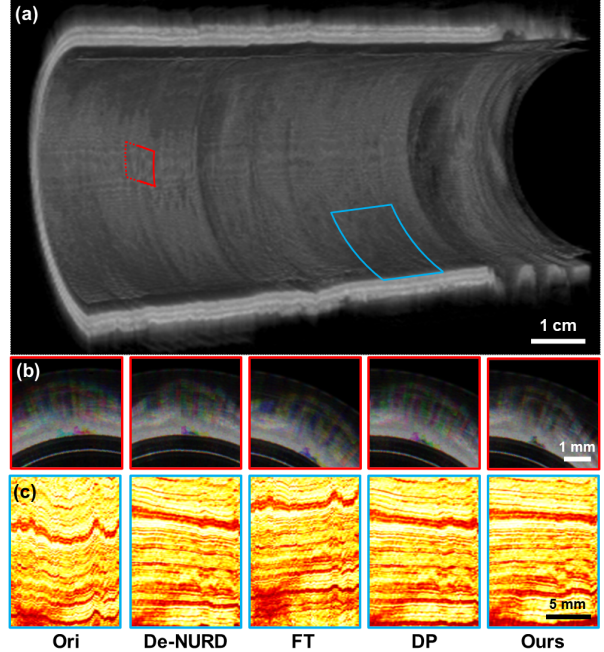


Fig. 4. Qualitative comparison of different NURD correction methods on open-source test data. (a) is the 3D view of a volumetric scan of gastrointestinal tract. The red and blue boxes refer to the zoom-in area in (b) and (c), respectively.

publicly-available datasets [4, 7, 8, 13, 16, 17] to train our model. As mentioned above, we use these data to generate the GT distortion vectors using the method in [10]. By applying these vectors to the B-scans, we create 20,000 original-distorted image pairs for the training. We then use another two publicly-available endoscopic datasets [13, 14] for evaluating our trained model, which they don't appear in training phase, as most AI studies do. Instead, we train our model in one go and evaluate on external test datasets. This can demonstrate the robustness of our approach and the generalization ability of the model. The two OCT open-source test datasets include gastrointestinal tract (648

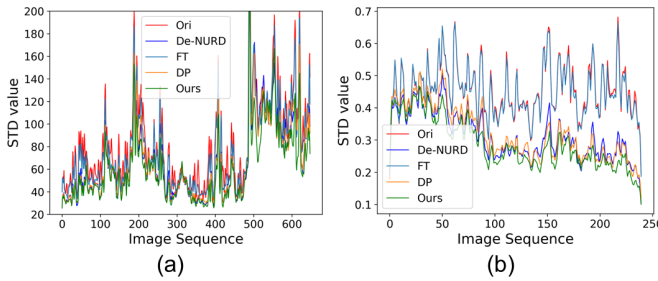


Fig. 5. Quantitative comparison of different NURD correction methods on open-source test data. (a) is the result of the gastrointestinal tract data. (b) is the result of the sponge surface data.

images) [13] and sponge surface (240 images) [14].

Figure 4 shows the qualitative comparison of different NURD correction methods on open-source test data. (a) is the 3D view of a volumetric scan of gastrointestinal tract. The red and blue boxes refer to the zoom-in area in (b) and (c), respectively. In Fig. 4(b), we use RGB channels to encode three consecutive frames. We can see our method achieves the best spatial consistency. In Fig. 4(c), we use mean value projection to obtain *en face* images. It can be seen that our method minimizes the distortion caused by NURD.

Figure 5 presents the quantitative comparison of different NURD correction methods on open-source test data. (a) and (b) are the results of the gastrointestinal tract and the sponge surface data, respectively. The results of our method are plotted in green, which demonstrates consistent minimum STD values over the image sequences.

We also evaluate the correction performance using a vessel

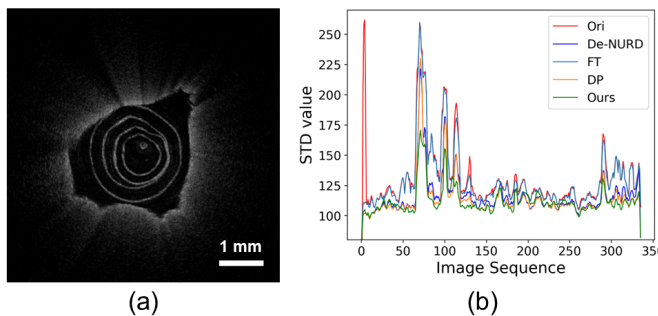


Fig. 6. Evaluation of the NURD correction performance on the data from our home-built endoscopic OCT system. (a) is an example of imaging vessel phantom. (b) is the quantitative comparison of different NURD correction methods using our private data.

phantom pull-back sequence (336 images) collected from our home-built endoscopic SD-OCT system (840 nm, 80kHz, 34 rps rotation speed). Figure 6(a) is an example of imaging vessel phantom. Figure 6(b) is the corresponding quantitative comparison of different NURD correction methods. We achieve minimal STD values throughout the image sequence.

Finally, we compare the processing speed of the two learning-based approaches in further detail. As shown in Table 1, our method achieves significant time-savings during pre/post-processing compared with the CNN-based method, which is due to the fact that our approach does not require the pre-

Table 1. Comparison of the processing speed using two learning-based methods.

Methods	pre- & post-processing	Model inference	Total time/frame	Frame per second
De-NURD	133.47±22.64 ms	3.11±1.68 ms	136.28±23.81 ms	8±1 fps
Ours	29.81±3.63 ms	8.86±0.48ms	38.67±3.64 ms	26±3 fps

construction of a correlation matrix.

In conclusion, we develop a cross-attention learning method, which enables real-time NURD correction in OCT. This method can be useful in many applications of endoscopic OCT and its functional extensions, such as surgical navigation and treatment monitoring.

Funding. This work was supported by the National Natural Science Foundation of China under Grant No. 51890892 and 62105198.

Disclosures. The authors declare no conflicts of interest.

Data availability. Data underlying the results presented in this paper are available in Ref. [4, 7, 8, 13, 14, 16, 17].

REFERENCES

1. E. A. Swanson and J. G. Fujimoto, *Biomed. optics express* **8**, 1638 (2017).
2. M. J. Gora, M. J. Suter, G. J. Tearney, and X. Li, *Biomed. optics express* **8**, 2405 (2017).
3. O. O. Ahsen, H.-C. Lee, M. G. Giacomelli, Z. Wang, K. Liang, T.-H. Tsai, B. Potsaid, H. Mashimo, and J. G. Fujimoto, *Opt. letters* **39**, 5973 (2014).
4. T. Wang, T. Pfeiffer, E. Regar, W. Wieser, H. van Beusekom, C. T. Lancee, G. Springeling, I. Krabbendam, A. F. van der Steen, R. Huber *et al.*, *Biomed. optics express* **6**, 5021 (2015).
5. W. C. Lo, N. Uribe-Patarroyo, K. Hoebel, K. Beaudette, M. Villiger, N. S. Nishioka, B. J. Vakoc, and B. E. Bouma, *Biomed. Opt. Express* **10**, 2067 (2019).
6. G. van Soest, J. G. Bosch, and A. F. van der Steen, *IEEE Trans. on Inf. Technol. Biomed.* **12**, 348 (2008).
7. Y. Miao, J. J. Jing, and Z. Chen, *Biomed. Opt. Express* **12**, 2508 (2021).
8. N. Uribe-Patarroyo and B. E. Bouma, *Opt. letters* **40**, 5518 (2015).
9. S. Guo, S. Wei, S. Lee, M. Sheu, S. Kang, and J. U. Kang, *IEEE J. Transl. Eng. Health Med.* **7**, 1 (2019).
10. G. Liao, O. Caravaca-Mora, B. Rosa, P. Zanne, D. Dall'Alba, P. Fiorini, M. de Mathelin, F. Nageotte, and M. J. Gora, *Med. Image Anal.* **77**, 102355 (2022).
11. A. Vaswani, N. Shazeer, N. Parmar, J. Uszkoreit, L. Jones, A. N. Gomez, Ł. Kaiser, and I. Polosukhin, *Adv. neural information processing systems* **30** (2017).
12. N. Stiennon, L. Ouyang, J. Wu, D. Ziegler, R. Lowe, C. Voss, A. Radford, D. Amodei, and P. F. Christiano, *Adv. Neural Inf. Process. Syst.* **33**, 3008 (2020).
13. M. J. Gora, J. S. Sauk, R. W. Carruth, K. A. Gallagher, M. J. Suter, N. S. Nishioka, L. E. Kava, M. Rosenberg, B. E. Bouma, and G. J. Tearney, *Nat. medicine* **19**, 238 (2013).
14. G. Liao, O. Caravaca-Mora, B. Rosa, P. Zanne, A. Asch, D. Dall'Alba, P. Fiorini, M. de Mathelin, F. Nageotte, and M. J. Gora, *IEEE Trans. on Med. Robotics Bionics* **3**, 855 (2021).
15. J.-Y. Zhu, T. Park, P. Isola, and A. A. Efros, “Unpaired image-to-image translation using cycle-consistent adversarial networks,” in *Proceedings of the IEEE international conference on computer vision*, (2017), pp. 2223–2232.
16. C. Sun, F. Nolte, K. H. Cheng, B. Vuong, K. K. Lee, B. A. Standish, B. Courtney, T. R. Marotta, A. Mariampillai, and V. X. Yang, *Biomed. optics express* **3**, 2600 (2012).
17. S.-W. Lee, A. E. Heidary, D. Yoon, D. Mukai, T. Ramalingam, S. Mahon, J. Yin, J. Jing, G. Liu, Z. Chen *et al.*, *Biomed. optics express* **2**, 243 (2011).

FULL REFERENCES

1. E. A. Swanson and J. G. Fujimoto, "The ecosystem that powered the translation of oct from fundamental research to clinical and commercial impact," *Biomed. optics express* **8**, 1638–1664 (2017).
2. M. J. Gora, M. J. Suter, G. J. Tearney, and X. Li, "Endoscopic optical coherence tomography: technologies and clinical applications," *Biomed. optics express* **8**, 2405–2444 (2017).
3. O. O. Ahsen, H.-C. Lee, M. G. Giacomelli, Z. Wang, K. Liang, T.-H. Tsai, B. Potsaid, H. Mashimo, and J. G. Fujimoto, "Correction of rotational distortion for catheter-based en face oct and oct angiography," *Opt. letters* **39**, 5973–5976 (2014).
4. T. Wang, T. Pfeiffer, E. Regar, W. Wieser, H. van Beusekom, C. T. Lancee, G. Springeling, I. Krabbenbom, A. F. van der Steen, R. Huber *et al.*, "Heartbeat oct: in vivo intravascular megahertz-optical coherence tomography," *Biomed. optics express* **6**, 5021–5032 (2015).
5. W. C. Lo, N. Uribe-Patarroyo, K. Hoebel, K. Beaudette, M. Villiger, N. S. Nishioka, B. J. Vakoc, and B. E. Bouma, "Balloon catheter-based radiofrequency ablation monitoring in porcine esophagus using optical coherence tomography," *Biomed. Opt. Express* **10**, 2067–2089 (2019).
6. G. van Soest, J. G. Bosch, and A. F. van der Steen, "Azimuthal registration of image sequences affected by nonuniform rotation distortion," *IEEE Trans. on Inf. Technol. Biomed.* **12**, 348–355 (2008).
7. Y. Miao, J. J. Jing, and Z. Chen, "Graph-based rotational nonuniformity correction for localized compliance measurement in the human nasopharynx," *Biomed. Opt. Express* **12**, 2508–2518 (2021).
8. N. Uribe-Patarroyo and B. E. Bouma, "Rotational distortion correction in endoscopic optical coherence tomography based on speckle decorrelation," *Opt. letters* **40**, 5518–5521 (2015).
9. S. Guo, S. Wei, S. Lee, M. Sheu, S. Kang, and J. U. Kang, "Intraoperative speckle variance optical coherence tomography for tissue temperature monitoring during cutaneous laser therapy," *IEEE J. Transl. Eng. Health Med.* **7**, 1–8 (2019).
10. G. Liao, O. Caravaca-Mora, B. Rosa, P. Zanne, D. Dall'Alba, P. Fiorini, M. de Mathelin, F. Nageotte, and M. J. Gora, "Distortion and instability compensation with deep learning for rotational scanning endoscopic optical coherence tomography," *Med. Image Anal.* **77**, 102355 (2022).
11. A. Vaswani, N. Shazeer, N. Parmar, J. Uszkoreit, L. Jones, A. N. Gomez, Ł. Kaiser, and I. Polosukhin, "Attention is all you need," *Adv. neural information processing systems* **30** (2017).
12. N. Stiennon, L. Ouyang, J. Wu, D. Ziegler, R. Lowe, C. Voss, A. Radford, D. Amodei, and P. F. Christiano, "Learning to summarize with human feedback," *Adv. Neural Inf. Process. Syst.* **33**, 3008–3021 (2020).
13. M. J. Gora, J. S. Sauk, R. W. Carruth, K. A. Gallagher, M. J. Suter, N. S. Nishioka, L. E. Kava, M. Rosenberg, B. E. Bouma, and G. J. Tearney, "Tethered capsule endomicroscopy enables less invasive imaging of gastrointestinal tract microstructure," *Nat. medicine* **19**, 238–240 (2013).
14. G. Liao, O. Caravaca-Mora, B. Rosa, P. Zanne, A. Asch, D. Dall'Alba, P. Fiorini, M. de Mathelin, F. Nageotte, and M. J. Gora, "Data stream stabilization for optical coherence tomography volumetric scanning," *IEEE Trans. on Med. Robotics Bionics* **3**, 855–865 (2021).
15. J.-Y. Zhu, T. Park, P. Isola, and A. A. Efros, "Unpaired image-to-image translation using cycle-consistent adversarial networks," in *Proceedings of the IEEE international conference on computer vision*, (2017), pp. 2223–2232.
16. C. Sun, F. Nolte, K. H. Cheng, B. Vuong, K. K. Lee, B. A. Standish, B. Courtney, T. R. Marotta, A. Mariampillai, and V. X. Yang, "In vivo feasibility of endovascular doppler optical coherence tomography," *Biomed. optics express* **3**, 2600–2610 (2012).
17. S.-W. Lee, A. E. Heidary, D. Yoon, D. Mukai, T. Ramalingam, S. Mahon, J. Yin, J. Jing, G. Liu, Z. Chen *et al.*, "Quantification of airway thickness changes in smoke-inhalation injury using in-vivo 3-d endoscopic frequency-domain optical coherence tomography," *Biomed. optics express* **2**, 243–254 (2011).